JOURNAL OF MATERIALS SCIENCE **37** (2002) 4349–4360

Formation and properties of ZnO nano-particles from gas phase synthesis processes

H. KLEINWECHTER, C. JANZEN, J. KNIPPING, H. WIGGERS, P. ROTH
Institut für Verbrennung und Gasdynamik, Gerhard-Mercator-Universität Duisburg, 47048 Duisburg, Germany
E-mail: Roth@ivg.uni-duisburg.de

ZnO nano-particles have been synthesized in low pressure flow reactors utilizing $Zn(CH_3)_2$ as precursor. Two different synthesis routes have been employed. A low pressure flame reactor and a microwave reactor were used for synthesis of ZnO particle in $Zn(CH_3)_2$ doped $H_2/O_2/Ar$ flames and $Zn(CH_3)_2$ doped Ar/O_2 plasmas, respectively. The particle formation process has been investigated *in situ* by a particle mass spectrometer. Also, sampled powders have been investigated *ex situ* by means of FT-IR, XRD, TEM, and UV-VIS. For both synthesis routes nanometer sized ZnO particles were found with particle diameters in the range between 4 to 8 nm. In cases of the flame reactor the results suggest a strong influence of water on the particle formation process.

1. Introduction

The physical and chemical properties of nano-particles differ essentially from those of bulk material. Extensive scientific efforts have been taken to investigate the dependency of those properties on particle size and to utilize them for practical applications. A major goal for further improvements and utilization in industrial applications is the production of nano-particles with defined physical and chemical properties. Especially nanometer sized ZnO particles have been in the scope of a variety of scientific investigations due to their interesting size dependent optical and electrical properties [1, 2]. As a direct band gap semiconductor with a band gap near 3.3 eV ZnO possesses a potential as material for optics, uv-light emitting devices, varistors and gas sensors [3, 4]. A variety of different methods have been applied to produce either ZnO thin films or ZnO particles, e.g., rf-sputtering [5], spray pyrolysis [6], and chemical precipitation techniques [7].

Gas phase synthesis routes have successfully been applied for the production of nanometer sized particles in the past. These methods have in common, that the particle formation process takes place from a supersaturated vapor by nucleation and condensation leading to an aerosol with particles suspended in the gas phase. Several techniques have been employed for particle synthesis among which the synthesis in doped $H_2/O_2/Ar$ low pressure flat flames and doped O_2/Ar microwave plasmas have been proven to be suitable for the production of metal oxide particles with a narrow size distribution and high purity. Major advantages of these gas phase synthesis routes are the possibility of an easy upscale of the apparatuses in order to produce large amount of material and the applicability of measurement techniques for an online determination of particle sizes in the resulting aerosols. Especially the development of a particle mass spectrometer (PMS) and its successful application to doped $H_2/O_2/Ar$ low pressure flat flames not only resulted in a better understanding of the particle formation processes but also proved to be a reliable on-line monitor yielding the size distribution of particles in the flame aerosols. In the past, Lindackers *et al*. [8, 9] synthesized SiO_2, Al_2O_3, and SnO_2 particles in low pressure $H_2/O_2/Ar$ flames doped with SiH_4, $Al(CH_3)_3$, and $Sn(CH_3)_4$. They investigated the evolution of particles in the flames along the flow coordinate with a PMS and could successfully show the impact of pressure, precursor concentration, and gas composition on the formation process and the resulting particle size. Similar investigation has been carried out by Janzen *et al*. [10] who studied the formation of Fe_2O_3 Particles in $Fe(CO)_5$ doped $H_2/O_2/Ar$ flames. Both authors compared their measurement results with a theoretical model including the homogeneous reactions of the $H_2/O_2/Ar$ flame and particle growth by Brownian coagulation. The synthesis of nano-particles from microwave plasma was pioneered by Vollath and coworkers who showed the high potential of this synthesis route in several publications, e.g., [11, 12]. The method was successfully applied for the synthesis of e.g., ZrO_2, TiO_2 and Al_2O_3. Recently, Janzen *et al*. [13] adopted the PMS measurement technique to a similar microwave flow reactor and measured size distributions of Fe_2O_3 particles from $Fe(CO)_5$ doped O_2/Ar plasmas.

The goal of the present work was to investigate the formation of ZnO nano-particles by means of aerosol synthesis routes. These include the synthesis in doped $H_2/O_2/Ar$ flames as well as in doped O_2/Ar plasmas. Dimethylzinc ($Zn(CH_3)_2$) was used in both cases as the precursor material delivering zinc to the reaction gases. The main focus was set on the investigation of the particle formation process by measuring size distribution

with a PMS. Small amounts of particles were extracted out of the flame gases by different sampling methods and analyzed with respect to their physical and chemical properties. As deposition techniques, a thermophoretic sampler as well as an *in situ* sampling method were used. In the latter case, particles were deposited directly onto TEM grids out of a particle loaded molecular beam. TEM was used to identify the particle size and morphology as well as the crystallinity and composition by electron diffraction and EDX, respectively. Crystallinity was also investigated by XRD. The optical and electronic properties were measured by FT-IR and UV-VIS spectroscopy.

2. Experimental

The formation of ZnO nano-particles was investigated in two vacuum reactors, which are schematically shown in Fig. 1. In both cases, mixtures of $Zn(CH_3)_2$ vapor and Ar were prepared prior to the experiment by the partial pressure method. For this purpose, $Zn(CH_3)_2$ vapor was lead into a previously evacuated mixing vessel (not shown) which was afterwards filled up with Ar to a pressure of 1 bar. The maximum precursor concentration in the resulting gas mixture is limited by the $Zn(CH_3)_2$ vapor pressure (12 mbar at room temperature) and thus, mixtures of up to 1.2% of $Zn(CH_3)_2$ in Ar can be prepared. During an experiment the gas mixture is released from the mixing vessel and fed to the synthesis reactor through a mass flow controller.

For the particle formation in H_2/O_2/Ar flames, a reactor was used in a way that has been applied for the synthesis of oxidic nano-particles in the past [8]. The $Zn(CH_3)_2$/Ar precursor was added to the premixed H_2/O_2/Ar flame gases inside a water cooled burner head, which was specially designed for the combustion of highly reactive gases preventing any preliminary reactions inside the burner [8]. The H_2/O_2/Ar/$Zn(CH_3)_2$ mixture enters the combustion chamber through a porous bronze plate and a laminar flame establishes downstream of the burner head. The latter is moveably mounted inside the combustion chamber, so that the distance between the burner head and a particle probing device can be adjusted. For particle probing, the flame reactor is equipped with two sampling devices. A water cooled stainless steel plate which can be moved into the flame gases for thermophoretic sampling, and a differentially pumped molecular beam probing system which enables the nearby undisturbed extraction of a "particle loaded" molecular beam. In the latter case, the sample is rapidly expanded into the free molecular regime which leads to a temperature drop, thus freezing all chemical and physical processes almost completely. Due to the molecular beam technique the sampling can be regarded as non-intrusive. The "particle loaded" molecular beam is directed into the analysis chamber where the electrically charged particulate fraction can be analyzed be means of a particle mass spectrometer (PMS). The same molecular beam technique was also used to study the particle formation in Ar/O_2 microwave plasmas. In this case a synthesis reactor similar to the one used by Janzen *et al.* [13] was employed. It consists mainly of two concentrically arranged quartz glass tubes through which the various gas mixtures are introduced, and a microwave cavity where 2.45 MHz microwave radiation is coupled into the gas flow. The inner glass tube (∅ 5 mm) is used for the $Zn(CH_3)_2$/Ar precursor gas mixture and the outer tube (∅ 24 mm) for the premixed Ar/O_2 mixture. In contrast to the flame reactor the distance between the microwave source and the sampling nozzle is fixed to a constant distance of 45 cm.

In order to obtain *in situ* information about the particle mass or diameter, both synthesis reactors were equipped with a particle mass spectrometer, which is located inside the high vacuum chamber of the molecular

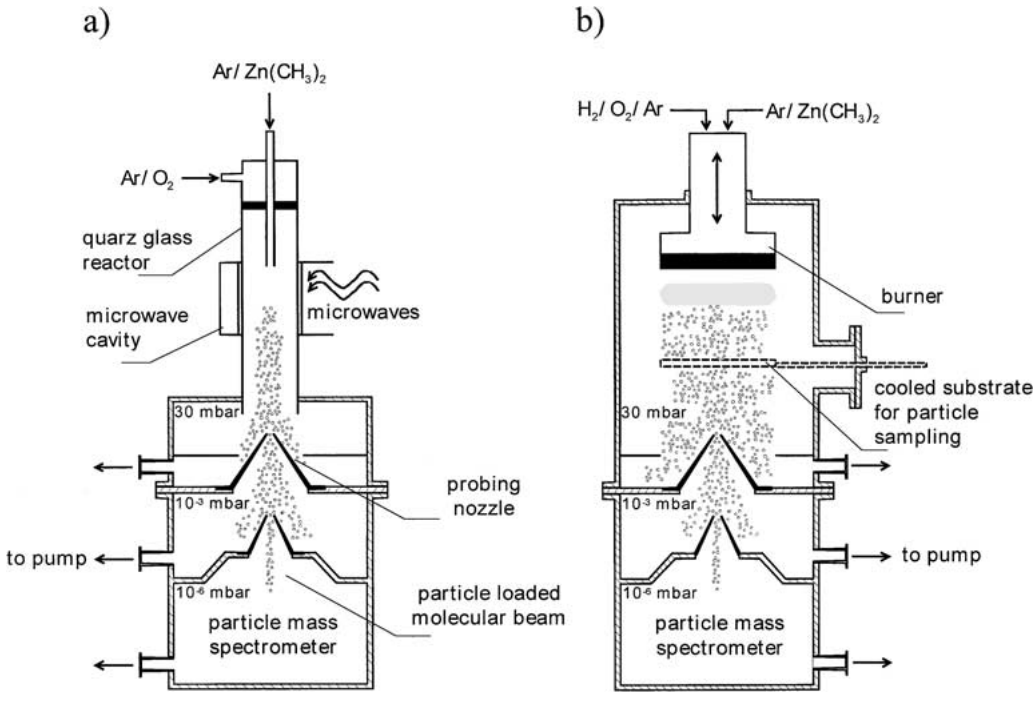

Figure 1 Experimental set-ups for the synthesis of ZnO nano-particles by (a) microwave reactor and (b) flame reactor. Both apparatuses were equipped with a molecular beam probing system and a particle mass spectrometer (PMS).

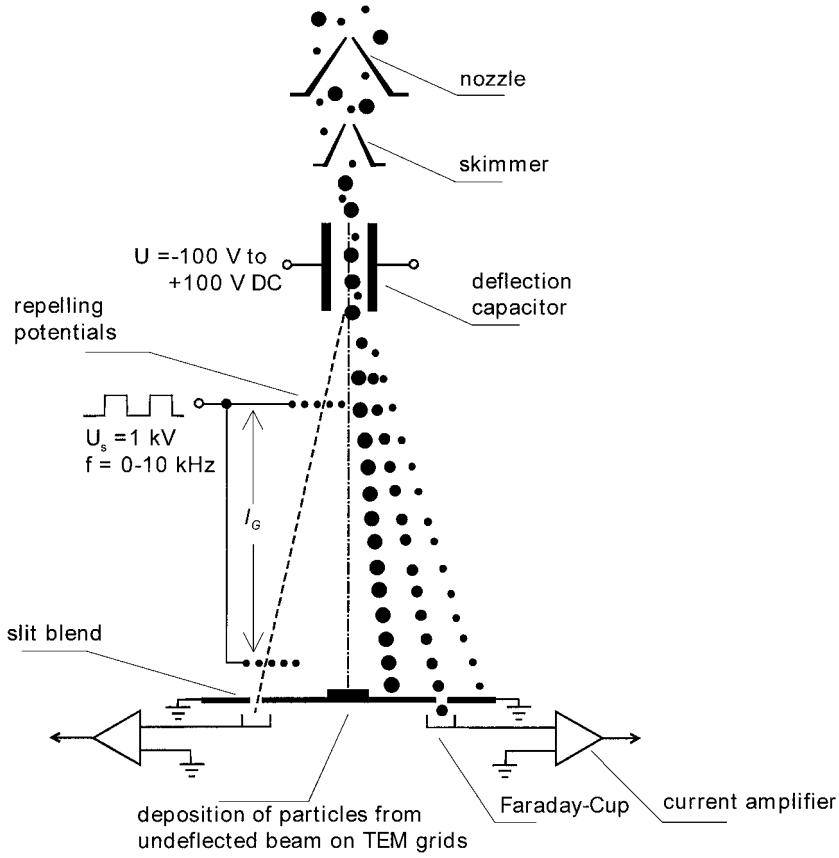

Figure 2 Schematic set-up of the particle mass spectrometer (PMS) with particle kinetic energy and particle velocity analyzer.

beam system. The basis of the particle mass spectrometer is the behavior of charged particles in an electric field. The principle of the PMS used has been described in detail [14]. According to Fig. 2, the main characteristics are as follows: the "particle loaded" molecular beam is directed through a capacitor which deflects the particles according to their kinetic energy and charge. The deflection voltage, the number of charges per particle, and the kinetic energy of the particles determine the deflection from the beam axis. Depending on the deflection voltage U_C, a certain part of the particles can pass through a slit located downstream the capacitor, delivering its charge to a Faraday-Cup, which is connected to an ultra-sensitive current amplifier. The relation between the deflection voltage U_C and the kinetic energy of the detected particles is

$$U_C = K_{\mathrm{PMS}} \frac{m_p}{ze} \frac{v_p^2}{2} \tag{1}$$

where m_p is the particle mass, v_p the particle velocity, and z the number of elementary charges e per particle. The constant in Equation 1 includes different geometrical and electrical parameters. The particle mass m_p can be determined from the deflection voltage provided that the velocity of the particles is known.

The setup shown on the left side of Fig. 2 is used to measure the required velocity of the particles. The selected beam of charged particles passes two grids supplied with a synchronously pulsed repelling potential. The upper grid forms packages of length l_p which depends on the frequency f of the grid voltage and the particle velocity v_p. Only very few or no particles can pass the second grid if the particle package length l_p is an odd-numbered multiple of the distance l_G between the grids. By changing the frequency of the deflection voltage U_C, a fluctuating particle current with maxima and minima is obtained. These minima and maxima of the particle current I_p obey the following conditions:

$$v_p = 2 \cdot f_{\mathrm{min},i} \cdot l_{p,i}$$

$$l_{p,i} = l_G, \frac{l_G}{3}, \frac{l_G}{5}, \text{etc} \tag{2}$$

Since it can be difficult to identify the first minimum which must be related to $l_{p,1} = l_G$, it can be shown that the difference between two minima is equal to $\Delta f_{\mathrm{min}} = 2 f_{\mathrm{min},1}$. Thus, Equation 3 reduces to:

$$v_p = \Delta f_{\mathrm{min}} \cdot l_G \tag{3}$$

Combination of Equation 1 and 3 leads to

$$U_C = \mathrm{const} \frac{m_p}{ze} \tag{4}$$

The resulting signals are current/voltage spectra of the kinetic energy of the particles. It has been shown that the current/voltage spectra are not equal to the probability density function (*PDF*) of the particle mass, because the sensitivity of the PMS depends on the deflection voltage [14]. The following relation between the measured particle current, the deflection voltage U_C, and the *PDF* is valid:

$$PDF(m_p) = \mathrm{const.} \frac{I(U_C)}{U_C} \tag{5}$$

Besides the PMS measurements, particles can be deposited on TEM grids located on the slit blend of the PMS. The deposition time varied between 15 and

90 minutes depending on the particle load in the reactive environment.

3. Results and discussion

3.1. $Zn(CH_3)_2$ doped H_2/O_2/Ar flames

In order to investigate the flame synthesis of ZnO particles, H_2/O_2/Ar flames were doped with $Zn(CH_3)_2$ in concentrations between 600 ppm and 3500 ppm. Since previous studies on the formation of oxidic nanoparticles in H_2/O_2/Ar flames revealed a strong influence of the precursor concentration on the resulting particle size, the goal of the first set of experiments was to elucidate the influence of this parameter on the formation of ZnO particles. All other parameters were kept constant and were adjusted to the following values: pressure $p = 30$ mbar, $H_2/O_2 = 1.69$, dilution gas ration $Ar/(H_2 + O_2) = 1.36$, velocity of the unburnt gases $v_u = 1.32$ m/s. These values were chosen from experiences of previous studies and they ensure a stable and laminar flame evolution as well as a high excess of oxygen for a complete oxidation of the precursor molecules. In order to extract sufficient amounts of particulate material for *ex situ* characterization, the cooled substrate was used for thermophoretic sampling. It was placed inside the flame gases at a distance of 60 mm above the burner head and was kept there for time periods of one to two hours during an experiment.

In contrast to the results of former studies of e.g., SiO_2 and Fe_2O_3 synthesis, no significant particle deposition could be observed on the substrate. Instead, a thin grayish film evolved that strongly adhered to the substrate. Only at the edges of the thermophoretic sampler and on much cooler reactor walls downstream of the substrate, a massive deposition of white particulate matter took place. This result could be observed during all experiments and did not change significantly with synthesis parameters or distance between burner head and substrate. From these observations it was obvious that no particle deposition took place on surfaces that were directly exposed to the hot flame gases. ZnO particles were only deposited on much cooler reactor walls, deduced from the characterization of the white powder fraction, which is discussed below.

The only meaningful explanation of this unexpected results is the assumption that ZnO is not stable under the conditions in the flame zone, which is characterized by high temperatures (T >1800 K) and high concentrations of the flame gas species H_2 and O_2 and the major reaction product H_2O. This assumption is supported by thermodynamic equilibrium calculations that were carried out with the FACT 3.05 program [15] assuming typical flame conditions und compositions of species. The essential result of this calculations was that the chemical equilibrium of this system was shifted to gaseous Zn for temperatures beyond 1500 K. Only for temperatures below 1300 K, ZnO is the predominant species besides H_2O, O_2 and Ar. Although this calculations can not account for the mostly kinetically controlled reactions in the flame zone, they strongly support the assumption that a formation of ZnO and thus particle nucleation in the flame core is unlikely. But this results can not explain the experimental observations alone, since the surface temperature of the substrate is expected to be much below 1300 K, even under the assumption that a thin deposited layer of particles thermally isolates the substrate and thus increase the surface temperature. Another superimposed effect might be related to reactions of ZnO with water molecules that are present in large quantities in the exhaust gases. In this context, studies on chemically induced sublimation of ZnO in H_2 and H_2O rich atmospheres at elevated temperatures (T >400 K) have been published [16, 17]. This effect was used for the synthesis of thin ZnO films by the so called close-spaced-vapor-transport technique and the authors took the following set of reactions into consideration:

$$\mathrm{ZnO(s) + H_2(g) \Leftrightarrow Zn(g) + H_2O(g)}$$

$$\mathrm{ZnO(s) + H_2O(g) \Leftrightarrow Zn(g) + H_2(g) + O_2(g)}$$

$$\mathrm{ZnO(s) + 2H_2O(g) \Leftrightarrow Zn(OH)_2 + H_2O(g)}$$

$$\mathrm{ZnO(s) + H_2O(g) \Leftrightarrow Zn(OH)_2.}$$

Although the details of the underlying chemistry is not known yet, these results emphasize an influence of water on the nucleation of ZnO particles during flame synthesis. The formation of intermediate products such as $Zn(OH)_2$ might play an important role which hinder the nucleation of ZnO particles. It is therefore evident that the concept of a nearby instantaneous oxidation of the metallic species in the flame gases, as it was assumed during the synthesis of SiO_2 or Fe_2O_3 in former studies, is not fulfilled in the case of Zn. Here, the particle formation process is predominantly influenced by a set of yet unknown homogeneous reactions, which have to be taken into account for a complete understanding of the process.

On the other hand, the deposition of a white powder fraction on much colder reactor walls showed, that the production of ZnO particles by flame synthesis is in principle possible, even though a complete understanding of the formation process has not been established yet. Such particles were redispersed in isopropanol and deposited on grids for TEM visualization. In Fig. 3, images of typical particles are shown. The detailed synthesis conditions are given in the figure caption. The particles are strongly agglomerated and a mean primary particle diameter of $d_p = 6.3$ nm was deduced from the images. EDX measurements revealed a composition of zinc and oxygen to equal amounts, emphasizing the presence of ZnO. This is also supported by electron diffraction results (see insert in the left image of Fig. 3), which clearly show the diffraction pattern of hexagonal ZnO (zincite). Complementary to this result the crystal structure was also investigated by means of X-ray diffraction, utilizing Cu K_α radiation. A typical example of a resulting diffraction pattern is shown in Fig. 4. Besides reflections of Al from the sample holder, the diffraction maxima of ZnO are clearly distinguishable. The relative broad peaks indicate the nano-crystalline nature of the particles and from the full width at half maximum, the mean crystalline size can be estimated in conjunction with Scherrer's equation [18]. For this purpose, the three most intense maxima were fitted to

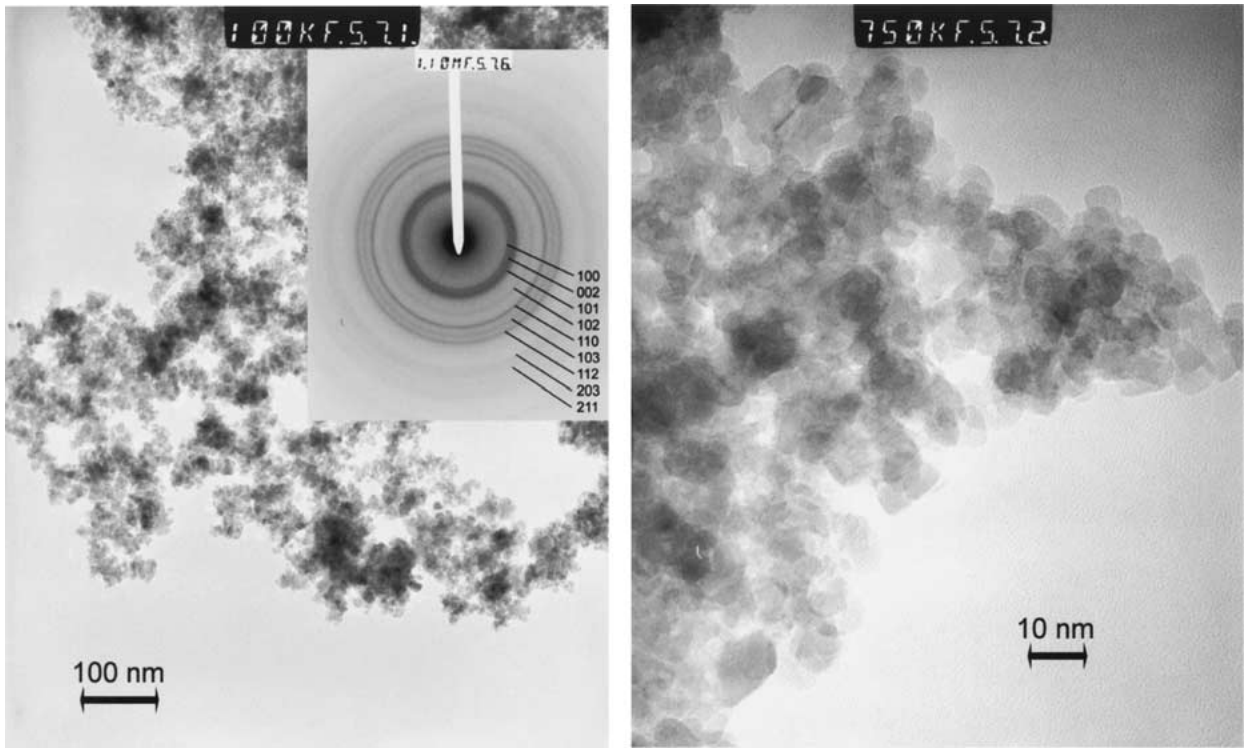

Figure 3 TEM images of ZnO nano-particles deposited on the reactor walls during flame synthesis. The insert in the left image shows the diffraction pattern of the particles. Synthesis conditions: $[Zn(CH_3)_2] = 1500$ ppm; $[H_2]/[O_2] = 1.69$; $[Ar]/[H_2] + [O_2] = 1.36$; $v_{an} = 1.32$ m/s; $p = 30$ mbar.

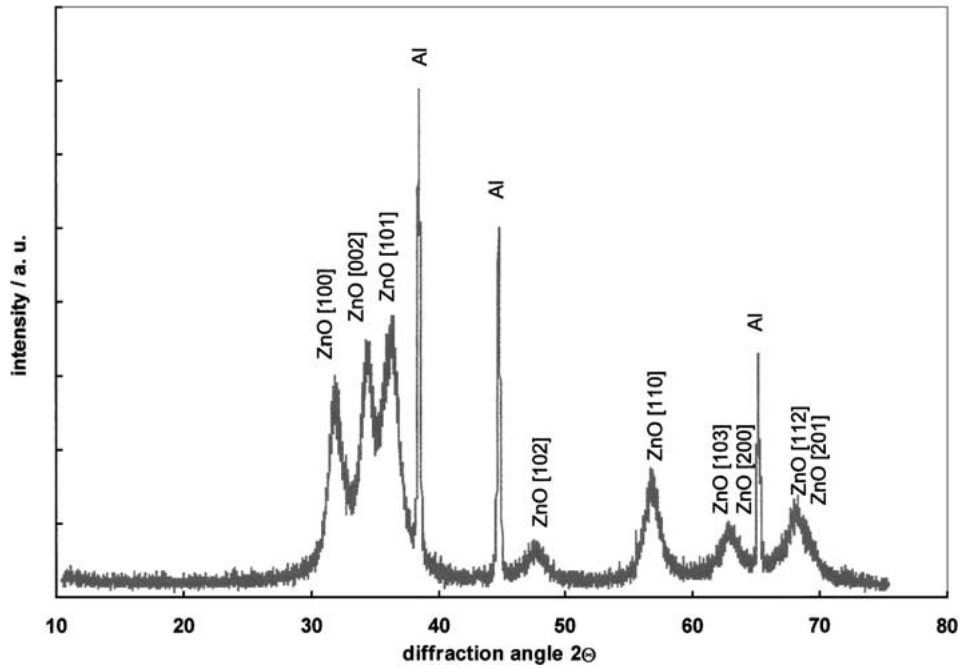

Figure 4 XRD pattern of ZnO nano-particles deposited on the reactor walls during flame synthesis. Synthesis conditions see Fig. 3.

Lorentz functions and their widths at half maximum were determined. In the case of the diffraction pattern shown in Fig. 4, this resulted in a mean crystallite size of 6.5 nm which corresponds well with the mean particle diameter obtained from TEM images (6.3 nm). This agreement indicates predominantly single crystalline primary particles.

Investigations of particles from different experiments with different precursor concentrations lead to similar results with respect to TEM and XRD analysis. The derived particle diameters are summarized in Table I. Also

TABLE I Specific surface area and diameter of ZnO particles obtained from flame synthesis with different precursor concentrations. Flame conditions: $[H_2]/[O_2] = 1.69$; $[Ar]/[H_2] + [O_2] = 1.36$; $v_{an} = 1.32$ m/s; $p = 30$ mbar

$[Zn(CH_3)_2]$ (ppm)	S_{BET} (m^2/g)	d_{pBET} (nm)	d_{pTEM} (nm)	d_{pXRD} (nm)
600	42.3	25.8	5.9	6.2
1500	46.8	23.3	6.3	6.5
2500	43.1	25.3	7.4	7.3
3500	43.4	25.1	8.5	8.3

shown are the specific surface areas of the powders, which were obtained from BET analysis [19]. The corresponding diameters d_{pBET} were derived from these values by assuming spherical particles. In all cases, a good agreement between mean diameters obtained from TEM images and those from XRD patterns were obtained. Both values show an increasing particle diameter with increasing precursor concentration. In contrast to this, the values derived from BET analysis resulted to much larger diameters and no clear influence of the precursor concentration can be seen. This discrepancy can be attributed to a partly coalescence of neighboring particles resulting in a sinter neck formation, which can be clearly seen from TEM images. Hence, the specific surface is strongly reduced compared to separated spheres and the calculated particle diameters are much bigger than the real primary particle size. From the fact that the specific surface area does not change significantly, although the primary particle diameter increases with increasing precursor concentration, a higher tendency for coalescence can be deduced for smaller particles.

In addition to particle size and crystal structure, the optical and electronic properties of ZnO particles are of particular interest. Therefore, the powders were also investigated by means of FT-IR and UV-VIS spectroscopy. In the infrared region ZnO usually shows distinct absorption bands around wavenumbers of 464 cm^{-1}. The position and number of these bands not only depend on crystal structure and chemical composition but also on particle morphology [20, 21]. Studies concerned with this morphology dependency have shown that in case of spherical ZnO particles, calculated as well as measured spectra show one distinct absorption maximum at around 464 cm^{-1} [22]. This maximum broadens and splits into two maxima if the particle morphology changes from spherical to a needle like shape. The latter is the preferred morphology from wet chemical synthesis routes under certain conditions and is the result of a preferred c-axis growth [22]. Therefore, reference spectra of ZnO powders often show two absorption maxima at around 512 cm^{-1} and 406 cm^{-1}, see e.g., [23]. Since the particle morphology from our flame syntheses is always nearby spherical, FT-IR measurements resulted always in spectra showing one distinct peak at around 462 cm^{-1}. A typical spectrum is given in Fig. 5. Besides the characteristic ZnO absorption, a maximum around 1631 cm^{-1} can be seen. It suggests the presence of hydroxyl groups, most likely present on the particle surface.

In order to obtain electronic properties of the particles, especially the band gap, UV-VIS spectroscopy has been employed. In the case of a direct band semiconductor like ZnO the absorption coefficient α is related to the excitation energy $h\nu$ by $\alpha = \text{const}\ (h\nu - E_g)^{0.5}$, where E_g is the band gap energy [24]. On the other hand, the absorption coefficient is also related to the measurable absorbance by the Lambert-Beer law: $\log(I_0/I_t) = \alpha d$, where I_0 and I_t are the intensities of the incident and transmitted light and d is the thickness of the absorbing layer. For excitation energies beyond the band gap energy, electron transitions from the valence to the conduction band result in a steep increase in the absorbance. The onset of the absorption can be obtained by plotting $\log^2(I_0/I_t)$ versus excitation energy $h\nu$ and a linear extrapolation to the energy axis gives E_g. In the present study, the diffuse reflection R was measured instead of the transmitted light and the relative absorbtance $A = \log(1/R)$ was taken as a measure for the absorption [25]. In order to estimate the band gap energy, A^2 was plotted versus $h\nu$ and the linear part was extrapolated to the energy axis. A typical example is given in Fig. 6, from which a band gap energy of $E_g = 3.24$ eV was obtained. Within the range of uncertainty of the method, this value agrees well with literature data for bulk ZnO of 3.3 eV [26]. Investigations of particles from experiments with different precursor concentrations lead to similar results and the derived band gap energies varied in the range between 3.24 eV and 3.28 eV. Particularly, no significant shift to larger band gap energies (blue-shift) was observed here. This

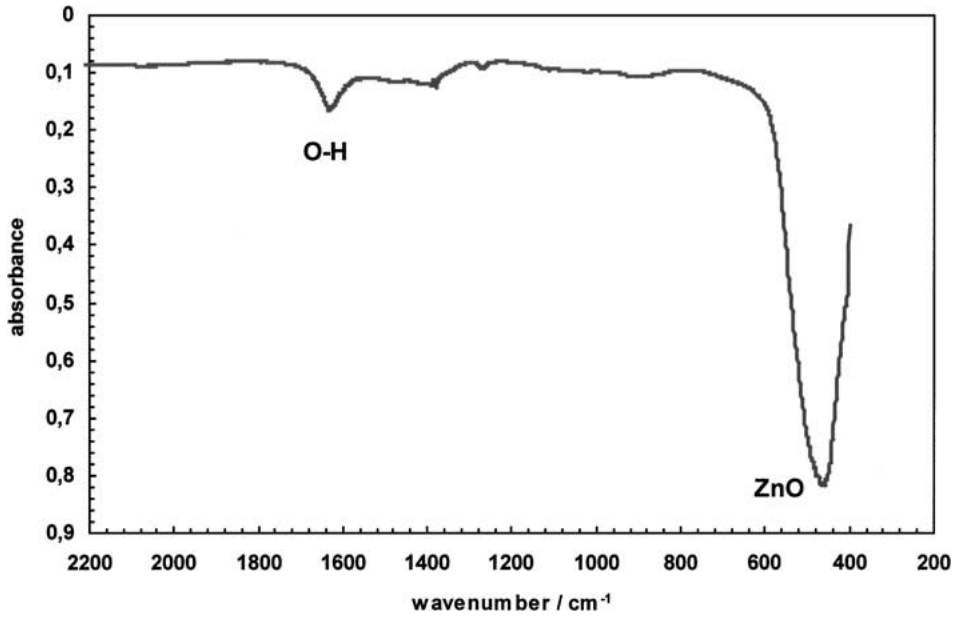

Figure 5 FT-IR spectrum of ZnO particles deposited on the reactor walls during flame synthesis. Synthesis conditions: $[Zn(CH_3)_2] = 600$ ppm; $[H_2]/[O_2] = 1.69$, $[Ar]/[H_2] + [O_2] = 1.36$; $v_{an} = 1.32$ m/s; $p = 30$ mbar.

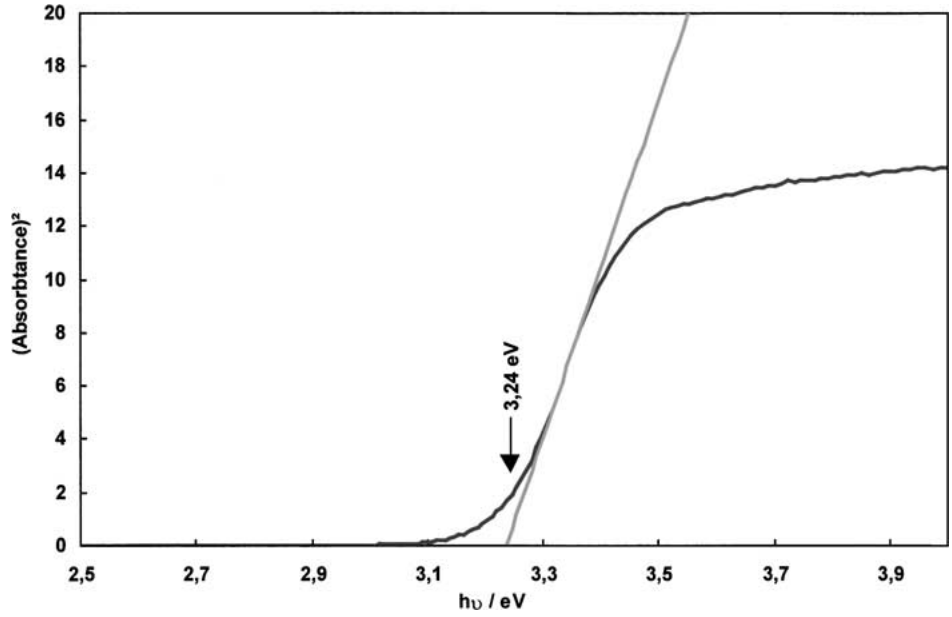

Figure 6 Determination of the band edge of ZnO particles deposited on the reactor walls during flame synthesis. Synthesis conditions see Fig. 5.

result must be assigned to the particle sizes between 5.9 nm and 8.5 nm, which are still to large for a significant blue-shift to occur. It is expected that this effect will be more pronounced for particle diameters below 5 nm.

Summarizing, the results of *ex situ* analysis of the wall deposited powders show that nano-crystalline ZnO particles were formed from $Zn(CH_3)_2$ doped $H_2/O_2/Ar$ flames. Due to the experimental observations, the formation process is not expected to start inside the hot flame core, as it was observed in former studies of e.g., SiO_2 or Fe_2O_3 particle synthesis. In the case of ZnO, particle nucleation probably takes place only after a sufficient cooling of the flame gases. This conclusion is also supported from PMS measurements, which never lead to a measurable particle current emphasizing the absence of particles in the hot flame gases.

3.2. $Zn(CH_3)_2$ doped Ar/O_2 microwave plasma

In contrast to the flame process, the microwave plasma enables a gas phase synthesis route at nearby water free conditions. Since the presence of water in combination with a high temperature reaction zone was assumed to prevent a ZnO particle formation in the flame gases, the microwave synthesis was expected to avoid this problem. Therefore, the experiments were focused primarily on the detection of particles in the plasma gases by means of particle mass spectrometry. In order to determine the influence of synthesis conditions on the measured size distributions, the precursor concentration, the microwave power, and the pressure were varied. All other parameters were kept constant at the following values: $[O_2]/[Ar] = 0.25$, velocity of the cold plasma gases $v_u = 1.32$ m/s.

The results of PMS measurements clearly indicated the nucleation of ZnO nano-particles in the plasma gases over a wide range of synthesis conditions. Typical PMS signals from an O_2/Ar plasma doped with 1061 ppm $Zn(CH_3)_2$ are shown in Fig. 7, where currents of positively and negatively charged particles are plotted versus the deflection voltage. The occurrence of particles of both polarities could be observed for all

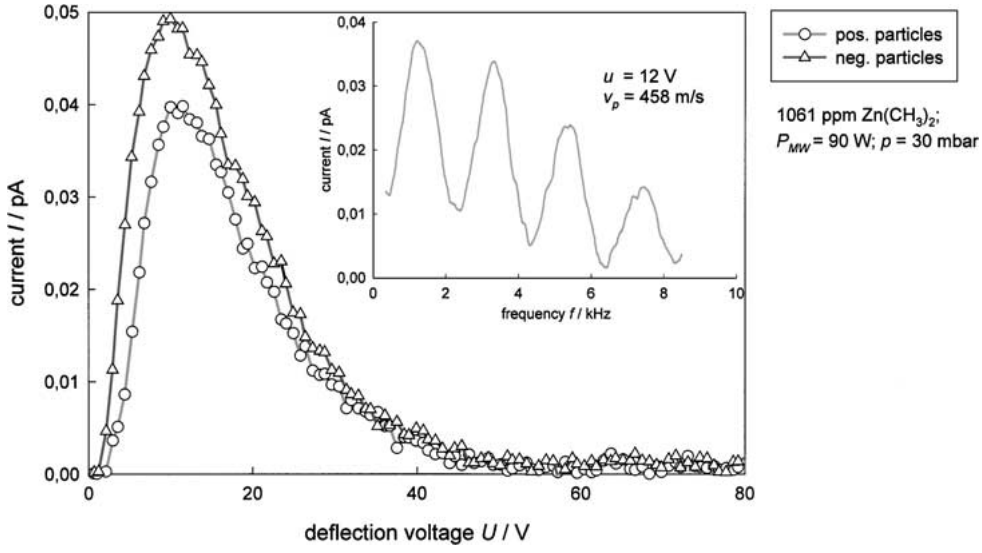

Figure 7 Typical current vs. voltage scan of positively and negatively charged particles obtained from PMS measurements during microwave synthesis. The insert shows the result of a particle velocity measurement.

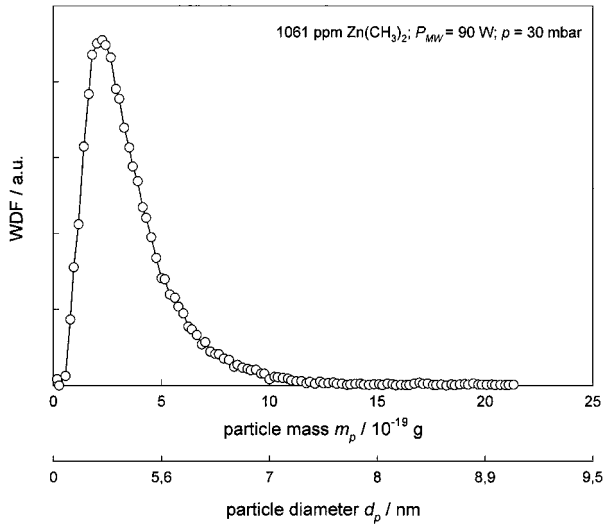

Figure 8 Probability density function (PDF) vs. particle mass calculated from the PMS measurement data shown in Fig. 7.

synthesis conditions, but the influence of the polarity on the derived mean particle sizes and widths of the size distributions was negligible. Therefore, the results shown in the following are limited to positively charged particles. From the fact that particles of both polarities were present in similar quantities, multiple charging of particles can already be excluded, since multiple charges are degraded immediately due to coulomb interactions with ions or particles of opposite polarity in a bipolar aerosol. Therefore, it was assumed that the particles carried only one elementary charge. In addition to the current/voltage spectra, a typical velocity measurement is also shown in Fig. 7 (see insert). The measurement was carried out at a deflection voltage of 12 V for positively charged particles und results in a particle velocity of 458 m/s. This value did not change significantly with deflection voltage or particle polarity. With the knowledge of the particle velocity and under the assumption of singly charged particles, mass distributions can be calculated from the current/voltage spectrum according to Equation 5. In Fig. 8, the resulting mass distribution calculated from the current/voltage spectrum of positively charged particles from Fig. 7 is shown. The distribution possesses the typical form of a lognormal distribution with one distinct maximum at $m_p = 2.3 \times 10^{-19}$ g. The corresponding diameter axis was calculated under the assumption of spherical particles and the density of bulk ZnO ($\rho = 5.5$ g/cm^3).

In addition to PMS measurements, particles were deposited from the undeflected molecular beam directly onto TEM grids. The goal of this experiments was a comparison between the size distributions derived from PMS measurements and those obtained from TEM analysis of the sampled particles. This comparison enables a direct verification of the PMS results and the assumptions concerning particle charge, morphology and density. In Fig. 9, TEM images of such particles are shown. The synthesis condition were the same as for the PMS measurements shown above. The image on the left hand side clearly shows the homogeneous particle distribution on the grid, whereas the image on the right hand side gives a magnified view of a selected area. Although the particles appear to form small islands on the grid, they are clearly separated from each other and possess a compact, almost spherical shape. The result of an image analysis is shown in the lower part of Fig. 9, where the histogram represents the relative frequencies of measured particle diameters. The comparison with

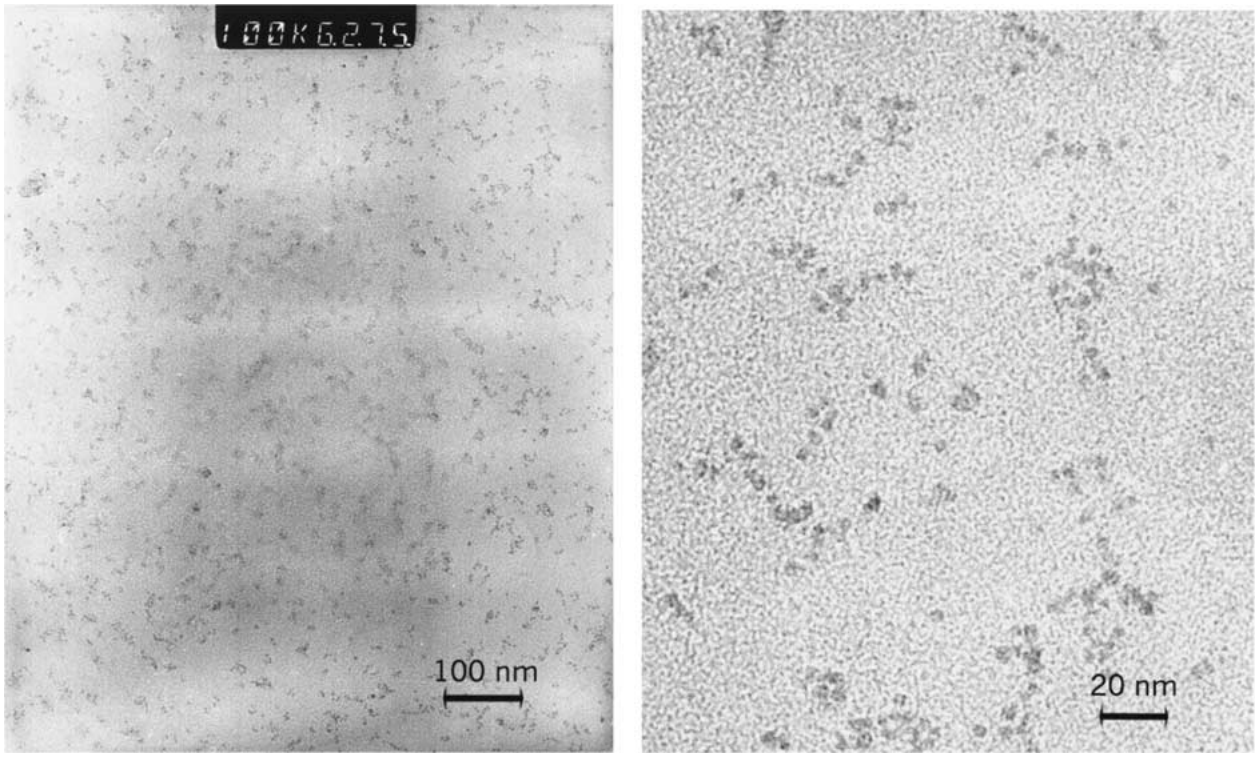

(a)

Figure 9 Comparison between PMS measurement and TEM image analysis of particles deposited directly from the undeflected molecular beam on TEM grids. (*Continued.*)

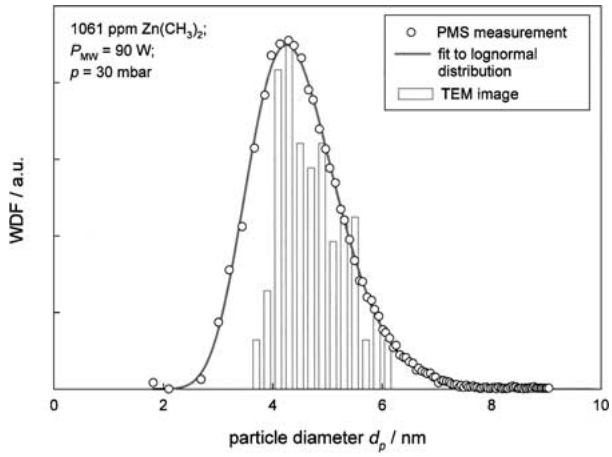

(b)

Figure 9 (*Continued*).

the size distribution derived from the PMS measurement is in excellent agreement confirming the assumptions made above. The mean diameter determined from the PMS measurement was $d_p = 4.4$ nm ($\sigma_g = 1.2$). The result of the image analyses deviates only slightly from this values with $d_p = 4.6$ nm and $\sigma_g = 1.14$. Since the amount of particles extracted from the molecular beam was usually very low ($\ll$1 mg) within reasonable sampling times, electron microscopy was the only possible technique for a further particle characterization. Here, electron diffraction was applied for the investigation of the crystalline structure. In the case of the sample shown in Fig. 9 these investigations did not result in reasonable diffraction patterns since the amount of collected particles on the grid was very low. Better results with respect to higher quantities were obtained for prolonged sampling periods. An extension from previously 15 min to 90 min resulted in the deposition of a nearly continues layer of ZnO particles, as shown in Fig. 10. Here, electron diffraction clearly reveals the crystalline structure of ZnO (see insert in Fig. 10) and it can therefore be assumed that the particles in the gas stream are already crystalline ZnO. In addition, this results also demonstrate the possibility for preparation of nano-crystalline particle layers with variable thickness by means of molecular beam particle deposition technique (MBPDT). In conjunction with PMS measurements, this technique offers the advantage of a very accurate prediction of the crystalline sizes within the layers.

The further experimental investigations were concerned with the influences of process parameters on the mean particle sizes. Three series of measurements were conducted with variable precursor concentration, pressure, and gas velocities. For each series, one parameter was varied systematically and size distributions were measured with the PMS, while the other

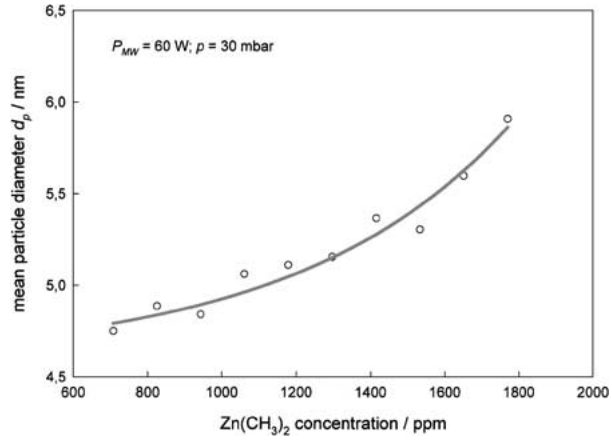

Figure 11 Influence of the precursor concentration on the mean particle diameter measured with the PMS in the microwave reactor flow.

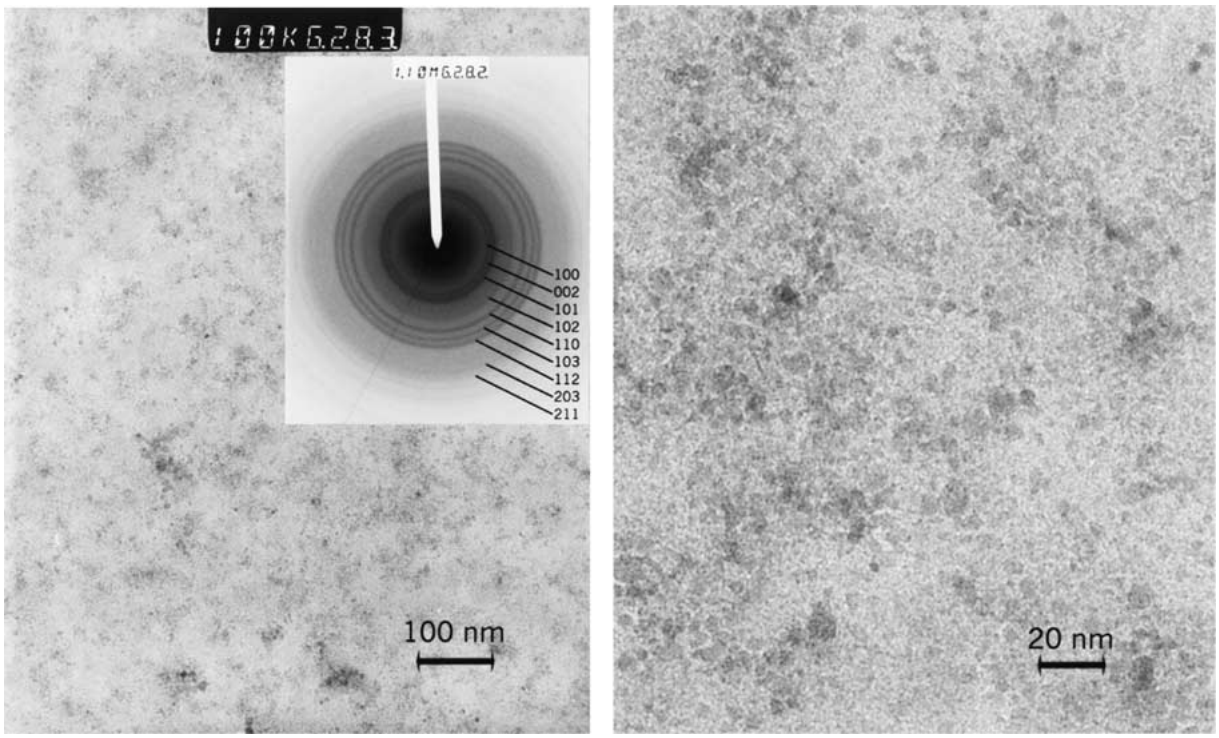

Figure 10 Nano-crystalline ZnO particle layer deposited on a TEM grid placed in the undeflected molecular beam during microwave synthesis. The insert in the left image shows the electron diffraction pattern which corresponds to crystalline ZnO.

parameters were kept constant. Since the distance between sampling nozzle and microwave cavity was fixed, all measurements represent the state of the particles in the flow 45 cm downstream of the plasma zone. In Figs 11 and 12, the mean particle diameters are shown as functions of precursor concentration and pressure, respectively. The geometric standard deviations of all distributions varied only slightly in the range between 1.18 and 1.26. During all experiments, the microwave power was 60 W. In the case of precursor concentration variation, the pressure was kept at 30 mbar and in the case of pressure variation, the precursor concentration was adjusted to 1061 ppm of $Zn(CH_3)_2$. As expected, an increase of one of the parameters resulted in an increasing particle diameter. This tendency can be explained by a higher coagulation and coalescence rate due to an increasing collision frequency between precursor molecules and particles, respectively. Although the trend of the data is obvious, the absolute values of the mean particle diameter vary only in a small range between 4.2 nm and 5.9 nm within the range of synthesis parameters applied. In a further series of experiments, the influence of the microwave power on the particle diameter was investigated. These measurements were carried out at a pressure of 30 mbar and a precursor concentration of 1061 ppm. In Fig. 13, the mean particle diameter is plotted versus microwave power. From this diagram, a clear tendency of a decreasing particle size with increasing power can be deduced. A possible explanation of this trend may be related to an accelerated flow at higher microwave powers. Since it can be expected, that the effective gas temperature increases with increasing microwave power, this leads to higher flow velocities for high microwave powers due to an expansion of the plasma gas. The higher velocity on the other hand leads to a reduced growth time of the particles, since the distance between sampling nozzle and microwave cavity is constant. This effect might explain the decreasing particle diameter. For further investigations of this trend and the particle growth process, a variable distance between microwave cavity and

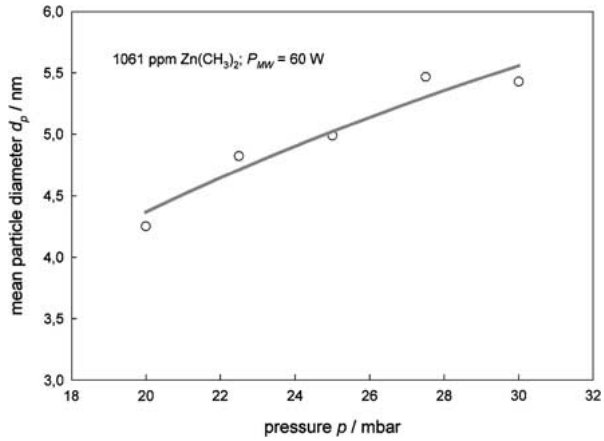

Figure 12 Influence of the reactor pressure on the mean particle diameter measured with the PMS in the microwave reactor flow.

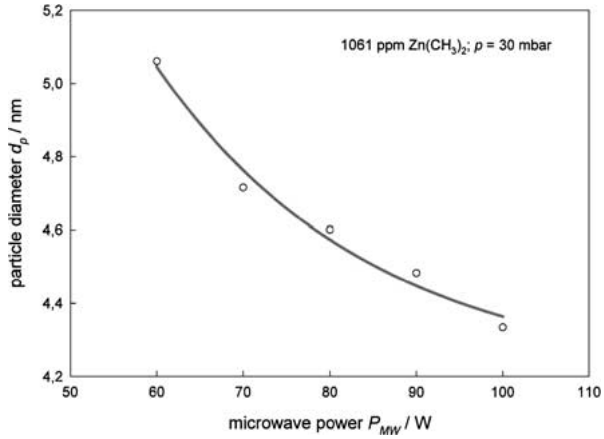

Figure 13 Influence of microwave power on the mean particle diameter measured with the PMS in the microwave reactor flow.

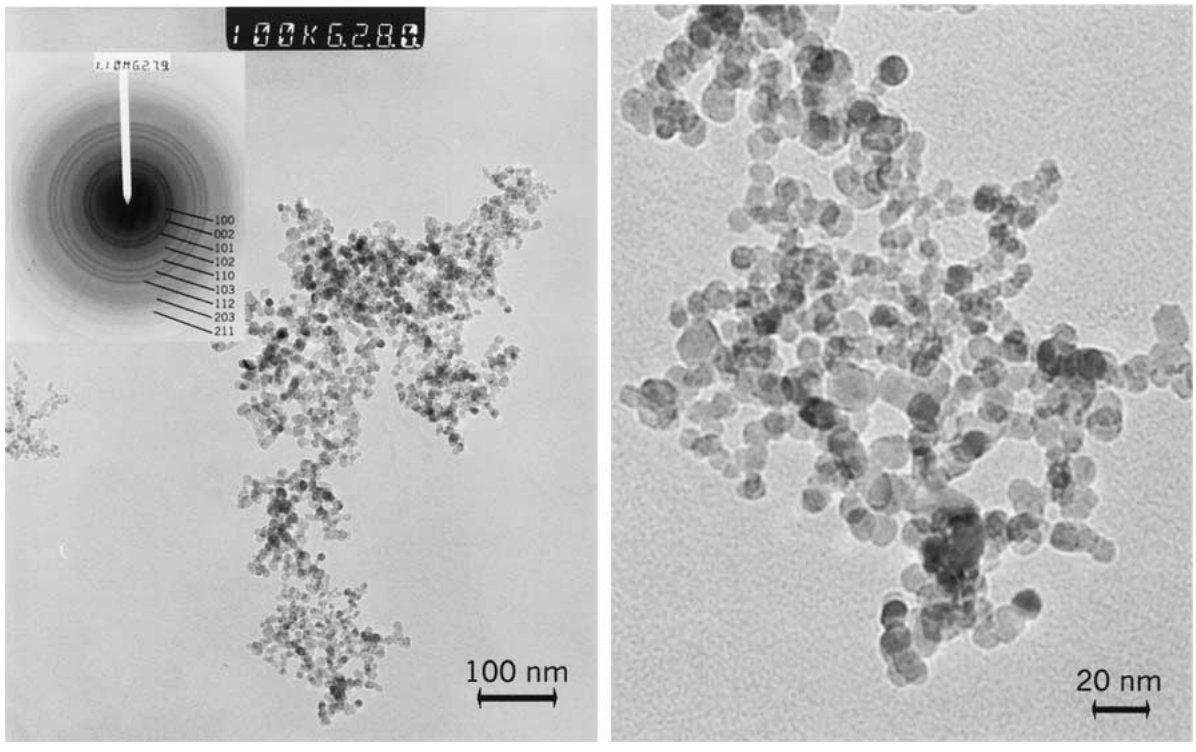

Figure 14 TEM images of ZnO nano-particles deposited on the quartz glass wall of the microwave reactor downstream of the microwave cavity.

sampling nozzle is necessary and will be implemented for future experiments.

In order to characterize microwave synthesized ZnO particles with respect to their optical and electronic properties, particles deposited at the wall of the quartz glass tube were investigated by means of TEM, XRD, FT-IR, and UV-VIS. The particles taken were deposited downstream of the microwave cavity, approximately at the height of the sampling nozzle. A fraction of such particles, which were dispersed in isopropanol and deposited on TEM grids. are shown in Fig. 14. The synthesis conditions were the same as for the particles shown in Fig. 9, which were sampled from the molecular beam. As can be seen from the insert in the left image, the particles consist of crystalline ZnO but their size is much bigger compared to the molecular beam sampled fraction. Here, the mean diameter deduced from the TEM images was $d_p = 10.3$ nm which is more than double the value of the molecular beam sampled particles ($d_p = 4.6$ nm). Thus, a further growth of deposited particles in the reactive plasma gas stream must be assumed. In order to sample higher amounts of particulate matter with properties representative to the gas born particles, an advanced sampling technique like an electrostatic or thermophoretic method is necessary. The further investigations of the deposited particles by means of XRD, FT-IR, and UV-VIS lead to almost the same results as for the wall deposited particles from flame synthesis and are therefore not shown here. In particular, the estimation of the band gap energy from UV-VIS measurements resulted to $E_g = 3.28$ eV which is again close to the value of bulk ZnO.

4. Conclusions

Gas phase synthesis routes have been proven to be suitable techniques for the production of oxidic nanopaticles. In this work, the formation of ZnO particles was investigated in doped $H_2/O_2/Ar$ low pressure flames as well as in doped O_2/Ar microwave plasmas. In both cases the liquid precursor $Zn(CH_3)_2$ was used as dopant, which was evaporated and premixed with the flame or plasma gases, respectively. Both synthesis reactors were equipped with a molecular beam sampling system, which enables a "non-intrusive" extraction of "particle-loaded" molecular beam from the exhaust gases and size distribution measurements in conjunction with a particle mass spectrometer (PMS).

The results of the flame synthesis suggest that particle nucleation inside the hot reaction zone is not probable. Neither the attempt to sample particles thermophoretically nor the extraction by the molecular beam technique indicated the existence of particles in the flame core. Particularly, no particles could be detected with the PMS. Only on much cooler reactor walls a deposition of crystalline ZnO particles has been observed, which showed primary particle diameters in the range between 6.2 nm and 8.2 nm. Here, an increasing particle size with increasing precursor concentration could be observed. Fractions of these particles were investigated by means of TEM, XRD, FT-IR, and UV-VIS. In all cases the particles were crystalline ZnO (zincite) and showed only one distinct absorption maximum in FT-IR spectra at around 462 cm^{-1}, which can be assigned to ZnO. Another maximum at around 1631 cm^{-1} suggests the presence of hydroxyl groups. From UV-VIS measurements band gap energies were estimated to values between 3.24 and 3.28 eV.

In opposite to the flame process a nucleation of ZnO particles in the plasma gases could be observed during microwave synthesis, and size distributions were measured with the PMS for different synthesis conditions. Furthermore, particles were sampled from the molecular beam directly on TEM grids for a comparison with PMS distributions. By this technique nanocrystalline ZnO particle layers with a variable thickness were deposited depending on sampling duration. The sizes of the deposited particles were in excellent agreement with size distributions from PMS measurement. Mean particle diameters in the range between 4.2 nm and 5.9 nm were measured depending on the synthesis conditions. As can be seen from the flame synthesis, not only kinetic properties of the particle formation but also thermodynamic considerations must be taken into account. Microwave plasma synthesis is a suitable method to overcome difficulties, which arise from particle formation in a chemically heated rector. The instrumental equipment used enables us to choose between chemical and physical energy addition for a better understanding of particle formation processes.

Acknowledgements

Financial support of the German Science Foundation (DFG) is gratefully acknowledged. The authors would like to thank Mr. H. Zähres for help with the TEM analysis.

References

1. S. MONTICONE, R. TUFEEU and A. V. KANAEV, *J. Phys. Chem.* B **102** (1998) 2854.
2. D. ZAHO and X. PAN, *J. Vac. Sci. Technol.* B **12**(5) (1994) 2880.
3. R. N. VISWANATH, S. RAMASAMY, R. RAMAMOORTHY, P. JAYAVEL and T. NAGARAJAN, *Nanostruct. Mater.* **6** (1995) 993.
4. A. P. CHATTERJEE, P. MITRA and A. K. MUKHOPADHYAH, *J. Mater. Sci.* **34** (1999) 4225.
5. A. BARKER, S. CROWTHER and D. REES, *Sens. Actuators* A **58**(3) (1997) 229.
6. Y. LEE, H. KIM and Y. ROH, *Jpn. J. Appl. Phys.* **40** (2001) 2423.
7. J. E. RODRIGUEZ-PAEZ, A .C. CABALLERO, M. VILLEGAS, C. MOURE, P. DURAN and J. F. FERNANDEZ, *J. Euro. Ceram. Soc.* **21**(7) (2001) 925.
8. D. LINDACKERS, M. G. D. STRECKER, P. ROTH, C. JANZEN and S. E. PRATSINIS, *Combust. Sci. Tech.* **123** (1997) 287.
9. D. LINDACKERS, C. JANZEN, B. RELLINGHAUS, E. F. WASSERMANN and P. ROTH, *Nanostruct. Mater.* **10**(8) (1998) 1247.
10. C. JANZEN and P. ROTH, *Combust. Flames* **125** (2001) 1150.
11. D. VOLLATH, *J. Mater. Res.* **8** (1993) 2978.
12. D. VOLLATH and D. V. SZABO, *J. Euro. Ceram. Soc.* **17** (1997) 1317.
13. C. JANZEN, H. WIGGERS, J. KNIPPING and P. ROTH, *J. Nanosci. Nanotech.* **1** (2001) 221.
14. P. ROTH and A. HOSPITAL, *J. Aeros. Sci.* **25** (1994) 61.
15. J. REICH, personal communication.
16. J. M. NTEP, M. BARBÉ, G. COHEN-SOLAL, F. BAILLY, A. LUSSON and R. TRIBOULET, *J. Cryst. Growth* **184/185** (1998) 1026.

17. R. TRIBOULET, J. M. NTEP, M. BARBÉ, P. LEMASSON, I. MORA-SERO and V. MUNOZ, *ibid.* **198/199** (1999) 968.
18. E. F. KAELBE, (ed.) "Handbook of X-Rays" (McGraw-Hill, New York, 1967).
19. S. BRUNAUER, P. H. EMMET and E. TELLER, *J. Amer. Chem. Soc.* **60** (1983).
20. F. A. SIGOLI, M. R. DAVOLOS and M. JAFELICCI, *J. Alloys Comp.* **262/263** (1997) 292.
21. S. HAYASHI, N. NAKAMORI and H. KANAMORI, *J. Phys. Soc. Jap.* **46**(1) (1979) 176.
22. M. ANDRÉS VERGÉS, A. MIFSUD and C. J. SERNA, *J. Chem. Soc. Farady Trans*, **86**(6) (1990) 959.
23. "The Infrared Spectra Handbook of Inorganic Compounds" Sadtler Research Laboraties (ed.) (Heyden & Son Ltd., London, 1984).
24. R. A. SMITH, "Semiconductors," 2nd ed. (Cambridge University Press, London, 1984).
25. J. F. CORDARO, in "Applied Spectroscopy," edited by J. Workman Jr. and A. Springsteen (Academic Press, London, 1998).
26. V. SRIKANT and D. R. CLARKE, *J. Appl. Phys.* **83**(10) (1998) 5447.

Received 22 November 2001
and accepted 3 June 2002